2-D Phase Demodulation for Deformable Fingerprint Registration

Zhe Cui, Jianjiang Feng, *Member, IEEE*, Shihao Li, Jiwen Lu, *Senior Member, IEEE*, and Jie Zhou, *Senior Member, IEEE*

***Abstract*— Fingerprint matching with elastic distortion is very challenging to deal with, and severe fingerprint distortion usually leads to false non-matches. This paper proposes a phase-based registration algorithm which can effectively eliminate the distortion between fingerprints and therefore is beneficial to the subsequent fingerprint matching. The key of the proposed algorithm is to reconstruct the distortion field through unwrapping phase difference between two fingerprints. Experiments on FVC2004, Tsinghua distorted fingerprint database, and NIST SD27 demonstrate that our algorithm outperforms other fingerprint registration methods and significantly improves matching accuracy.**

***Index Terms*— Fingerprint, distortion, matching, registration, phase unwrapping.**

I. Introduction

FINGERPRINT has been widely used in biometric authentication for its high accuracy and stable performances [1]. Although many matching algorithms have been published in the past forty years, most existing algorithms perform poorly for distorted fingerprints, as shown in the FVC2004 evaluation report [2]. Fingerprints distortion causes large changes of location of ridge pattern and minutiae, and thus strongly affects performances of fingerprint matching algorithms.

Since fingerprint distortion is highly elastic, rigid transformation based fingerprint registration cannot align two fingerprints accurately [3]–[5]. Thin-plate spline (TPS) model is thus introduced to solve this problem. Earlier research uses minutiae correspondences as landmark points to fit the model [6], [7]. However, when there exist some fake minutiae or the distorted region contains very few minutiae, TPS would fail to get a correct fitting result. Further improvement applies ridge curve correspondences instead of minutiae correspondences [8]. This method samples on ridge curves from matched minutiae pairs, and can generate more matching pairs than minutiae based method, which may make TPS fitting more precise. However, this improved method is still bothered by fingerprint distortion and noise since incorrect ridge pairs may lead to many incorrect point correspondences.

Recently, dense registration which uses block-based image correction method to generate dense matching points is introduced [9]. Dense registration method provides better registration results than minutiae-based methods, but correction operation used in this method is not robust to noises, and is of high computational cost.

Inspired by the concept and method of phase demodulation [10], we proposed a 2D phase demodulation algorithm for deformable registration of fingerprints. While 1D phase demodulation is well researched in communication area and some papers on 2D phase demodulation has been published in stereo matching area [11]–[13], but it has not been extended to fingerprint registration before. Fingerprints contain strong texture features, singular points, and noises, which are quite different from communication signal and natural images, and need specialized solutions when applying phase demodulation.

Through our algorithm, fingerprints are first coarsely registered by minutiae-based TPS registration and then finely registered by phase-based method (see Fig. 1). Therefore, the proposed method combines the advantages of minutiae based registration method which decreases distortion at global level, as well as the advantages of phase-based registration method which deals with local distortion and is of high robustness and fast speed. We thoroughly evaluate our algorithm both on registration error and matching accuracy. Experimental results on FVC2004 [14], Tsinghua Distorted Fingerprint (TDF) database [9] and latent fingerprint database NIST SD27 show that the proposed phase-based method outperforms minutiae-based methods and image block based method.

The following parts of this paper are organized as follows. Section II introduces the basic idea and approaches of phase demodulation, as well as the concept and meaning

Manuscript received November 20, 2017; revised April 18, 2018; accepted May 17, 2018. Date of publication May 29, 2018; date of current version June 15, 2018. This work was supported in part by the National Natural Science Foundation of China under Grants 61622207 and 61527808 and in part by the Shenzhen Fundamental Research Fund (subject arrangement) under Grant JCYJ20170412170438636. The associate editor coordinating the review of this manuscript and approving it for publication was Dr. Karthik Nandakumar. *(Corresponding author: Jianjiang Feng.)*

Z. Cui, S. Li, J. Lu, and J. Zhou are with the State Key Laboratory of Intelligent Technologies and Systems, Department of Automation, Tsinghua University, Beijing 100084, China, and also with the Beijing National Research Center for Information Science and Technology, Tsinghua University, Beijing 100084, China (e-mail: phy_cuiz10@163.com; li_sh10@foxmail.com; lujiwen@tsinghua.edu.cn; jzhou@tsinghua.edu.cn).

J. Feng is with the State Key Laboratory of Intelligent Technologies and Systems, Department of Automation, Tsinghua University, Beijing 100084, China, with the Beijing National Research Center for Information Science and Technology, Tsinghua University, Beijing 100084, China, and also with the Graduate School at Shenzhen, Tsinghua University, Shenzhen 518055, China (e-mail: jfeng@tsinghua.edu.cn).

This paper has supplementary downloadable material available at http://ieeexplore.ieee.org., provided by the authors. The material includes experiment results of MCC matcher. Contact jfeng@tsinghua.edu.cn for further questions about this work.

Color versions of one or more of the figures in this paper are available online at http://ieeexplore.ieee.org.

Digital Object Identifier 10.1109/TIFS.2018.2841849

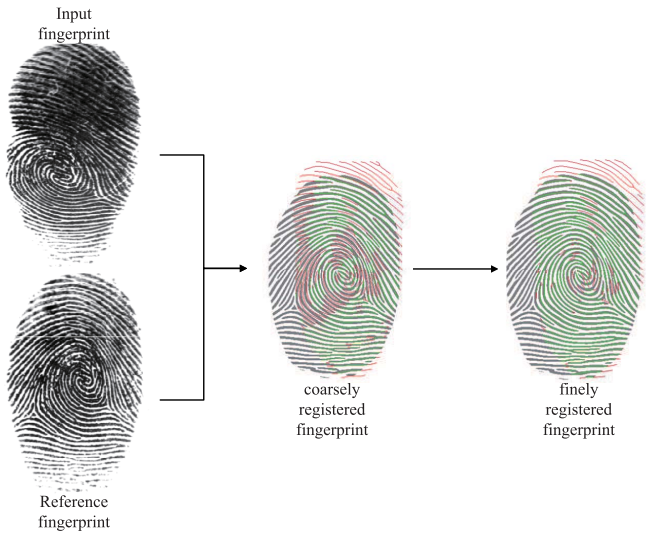

Fig. 1. Our registration method consists of two major steps: minutiae based coarse registration and phase based fine registration.

of phase unwrapping. Section III explains the main steps of the proposed method, including four parts: feature extraction, initial registration, phase unwrapping, and fine registration. Section IV shows the experiment results of the proposed method regarding registration accuracy, matching accuracy and efficiency. Section V concludes the paper and summarizes our method.

II. Image Distortion Field Estimation Based on 2-D Phase Demodulation

A. Phase Modulation and Demodulation

Phase modulation (PM) is an important signal modulation method in signal processing, and has been successfully applied in wireless communications. Modulation is to transfer message signal by modulating message onto carrier signal, and demodulation is to recover the message signal from the received modulated signal, as shown in Fig. 2. Let $s_m(t)$ be the message signal, $s_c(t) = A\cos\omega_c t$ be the carrier signal, then the phase modulated signal $s_{PM}(t)$ is [10]

$$s_{PM}(t) = A\cos(\omega_c t + K_{PM} s_m(t)), \tag{1}$$

where A and K_{PM} are parameters. As for demodulation, the received signal $s_{PM}(t)$ is multiplied by the carrier signal delayed by $\pi/2$,

$$\begin{aligned} s_{PD}(t) &= -A\sin\omega t\cos(\omega_c t + K_{PM} s_m(t)) \\ &= \frac{A}{2}\left(\sin(K_{PM} s_m(t)) - \sin(2\omega_c t + K_{PM} s_m(t))\right). \end{aligned} \tag{2}$$

Then $s_{PD}(t)$ is sent into a low-pass filter to separate $s_f = \sin(K_{PM} s_m(t))$ from $s_{PD}(t)$, and the local phase of $s_f(t)$ is just the message signal through Hilbert transform.

Phase method is later introduced into image registration area for its benefits of high robustness against noises and fast computational speed [15]. Corresponding to signal modulation situation, we can treat input image as the modulated signal, reference image as the carrier signal, and the target of image registration is to recover the distortion field as the message signal. Phase map of the image in frequency domain contains much valid information, and thanks to the Fourier Shift Theorem [16], phase differences between input and reference images also contain information of image distortion. Thus we can demodulate the distortion field from phase differences of the input and reference images.

Consider a single plane wave $f(x, y) = \exp(2\pi i u_0 x)$, and clearly its unwrapped continuous phase is $\Phi(x, y) = 2\pi u_0 x$. If the image is distorted according to some distortion field $T(x', y')$, the distorted sine wave is:

$$f_d(x, y) = \exp(2\pi i u_0 x'), \tag{3}$$

where $T(x', y')$ is the distortion function moving original point (x', y') to new position $(x, y) = (x' + T(x', y'), y')$. Here the distortion field T has only horizontal component for simplicity. Therefore, the distorted phase map is

$$\Phi_d(x, y) = 2\pi u_0 x' = 2\pi u_0 (x - T(x', y')), \tag{4}$$

and the phase difference $\Delta\Phi = \Phi_d - \Phi$ is

$$\Delta\Phi(x, y) = -2\pi u_0 T(x', y'). \tag{5}$$

Finally, the distortion field estimated from phase difference is

$$T_e(x, y) = -\frac{\Delta\Phi(x, y)}{2\pi u_0} = T(x', y'). \tag{6}$$

The estimation error is:

$$\begin{aligned} \delta_T(x, y) &= |T(x', y') - T(x, y)| \\ &\leqslant |x - x'| \max_{z\in[\min(x,x'),\max(x,x')]} \left|\frac{\partial T(z, y)}{\partial z}\right|. \end{aligned} \tag{7}$$

The distortion field is recovered with a deviation proportional to the distance between original position x' and new position x. As mentioned in the final paragraph of Section I, phase method is applied after coarse registration, which roughly aligns input and reference fingerprints. So the distorted point x is near original point x', their distance is small for further precise registration. Based on this prior knowledge, we can assert that the estimation error δ_T can be neglected, phase method can fully recover the distortion field. Fig. 3 shows those two approaches, the top part is the image distortion route, and the bottom part is the phase shift route, where phase extraction and unwrapping are used. Both image distortion and phase shift routes generate almost the identical distorted result, they both have the ability to transform images.

Therefore, by extracting phase map and calculating unwrapped phase difference, we can rebuild the distortion field from the phase aspect. Fig. 4 shows an example procedure to compute distortion field by phase method. The original image is a standard plane wave that propagates to the right, and we have the distorted image needed to be finely registered. The target is to obtain the distortion field for fine registration. First, we extract the wrapped phase of original and distorted images and get their corresponding wrapped phases described in Section II-B. Then we subtract the two phases and get phase differences. From the two pictures of phase difference we can see that wrapped phase difference has abrupt changes,

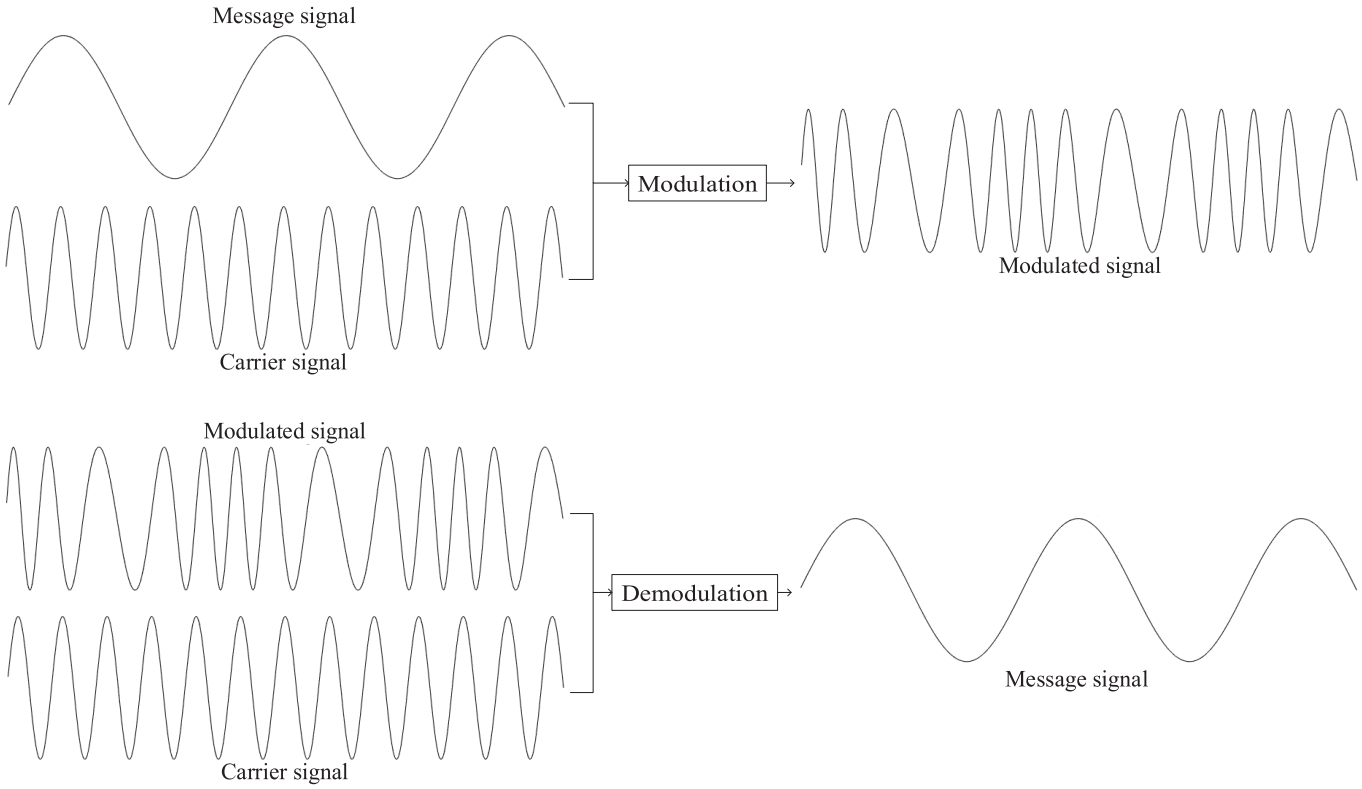

Fig. 2. Signal modulation and demodulation.

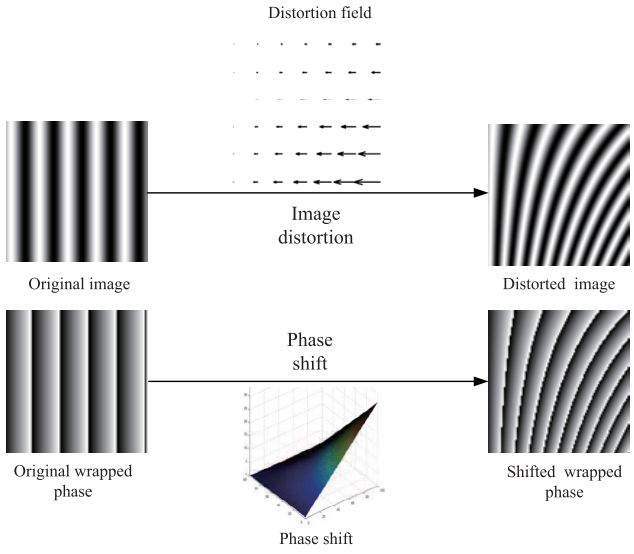

Fig. 3. Demonstration of the equivalence between image distortion and phase shift. The image distortion route and the phase shift route get the same distorted result.

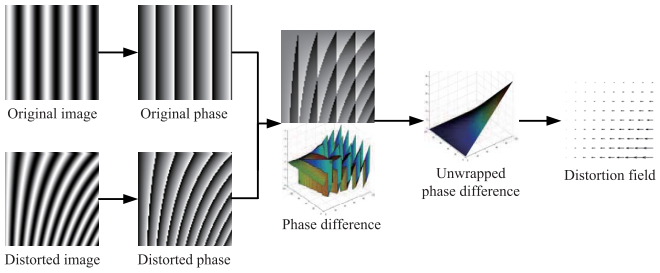

Fig. 4. Procedure of phase-based distortion field computation, assuming that the two input images have already been coarsely registered.

therefore, we apply phase unwrapping method in Section II-C to get the unwrapped phase difference. Finally, we can easily obtain the distortion field from unwrapped phase difference described in Section II-D.

B. Phase Extraction

Unlike most images, fingerprint images contain strong texture features generated by rugged finger skin. The distribution of valleys and ridges makes fingerprint images just similar to a 2-dimensional sine wave function. Larkin and Fletcher [17] introduce an amplitude and frequency modulated (AM-FM) function to describe fingerprints:

$$f(x, y) = a(x, y) + b(x, y)\cos[\Psi(x, y)] + n(x, y), \quad (8)$$

where $a(x, y)$ is the offset, $b(x, y)$ is the amplitude, $n(x, y)$ is the noise, and $\Psi(x, y)$ is the phase information. The most important item is the phase $\Psi(x, y)$, which controls ridge patterns of fingerprint. The offset $a(x, y)$, the amplitude $b(x, y)$ and the noise $n(x, y)$ only adjust brightness and contrast of the image, which makes the fingerprint image more real.

The phase information of 2-D images can be obtained through a 2-D complex Gabor filter [18], which can be viewed as the combination of sine wave with Gaussian

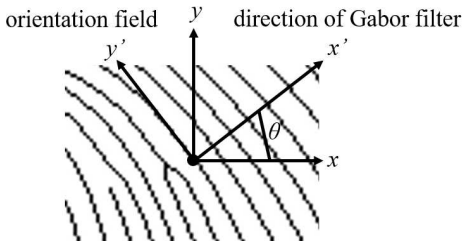

Fig. 5. Directions of original coordinates x, y and new coordinates x', y' rotated by angle θ. The direction of Gabor filter, or the new x', is set perpendicular to the orientation field, or y'.

envelope:

$$G(x, y) = \exp\left(-\left(\frac{x'^2}{2\sigma_x^2} + \frac{y'^2}{2\sigma_y^2}\right)\right)\exp(i(2\pi u_0 x' + \varphi)), \tag{9}$$

and x', y' is the original coordinates x, y rotated by angle θ,

$$\begin{pmatrix} x' \\ y' \end{pmatrix} = \begin{pmatrix} \cos\theta & \sin\theta \\ -\sin\theta & \cos\theta \end{pmatrix}\begin{pmatrix} x \\ y \end{pmatrix}. \tag{10}$$

Parameter θ controls rotation angle of Gabor filter $G(x, y)$, u_0 is the filtering frequency, σ_x and σ_y are the standard deviation of Gaussian distribution along x and y direction.

The complex Gabor filter $G(x, y)$ is an analytic signal and its real and imaginary components are corresponding functions through Hilbert transform, which is beneficial for estimating local amplitude and local phase. $G(x, y)$ is also a band-pass filter of main frequency u_0 based on its definition, and has high responses to local fringe pattern near frequency u_0. Therefore, $G(x, y)$ is very suitable for fingerprint patterns.

In fingerprint phase extraction, the frequency parameter u_0 and orientation parameter θ correspond to the frequency and direction of fingerprint ridge, and we use period map $P(x, y)$ and orientation field $O(x, y)$ to calculate these parameters:

$$\begin{aligned} u_0 &= 1/P(x_0, y_0), \\ \theta &= -\left\{O(x_0, y_0) + \frac{\pi}{2}\right\}, \end{aligned} \tag{11}$$

where $P(x_0, y_0)$ is the local ridge period at position (x_0, y_0) and $O(x_0, y_0)$ is the local ridge orientation at position (x_0, y_0). Period map $P(x, y)$ is the average distance between two adjacent ridges in the neighborhood of (x, y), and orientation field $O(x, y)$ is the orientation of the ridge at position (x, y), thus they can be used to measure the frequency and direction of the filter $G(x, y)$. Fig. 5 illustrates the relative directions of original coordinates x, y, the rotated coordinates x', y', the direction of orientation field $O(x, y)$, and the direction of Gabor filter $G(x, y)$.

C. Phase Unwrapping

Let $C_1(x, y)$ and $C_2(x, y)$ be the convolution product of image $I_1(x, y)$ and $I_2(x, y)$ with Gabor filter $G(x, y)$ respectively, then the local phase of $I_1(x, y)$ and $I_2(x, y)$ can be expressed as:

$$\begin{aligned} \phi_1(x, y) &= \text{atan2}(\text{Re}[C_1(x, y)], \text{Im}[C_1(x, y)]), \\ \phi_2(x, y) &= \text{atan2}(\text{Re}[C_2(x, y)], \text{Im}[C_2(x, y)]), \end{aligned} \tag{12}$$

where $\text{Re}[z]$ and $\text{Im}[z]$ are the real and imaginary components of complex signal z, and $\text{atan2}(x, y)$ is the four quadrant arctangent function returning the angle of complex number $x + yi$. Then the phase difference between $\phi_1(x, y)$ and $\phi_2(x, y)$ is:

$$\Delta\phi_{12}(x, y) = \phi_1(x, y) - \phi_2(x, y). \tag{13}$$

The phase difference by direct subtraction may have discontinuity at some points, generating a leap of 2π, as showed in Fig. 4. The aim of phase unwrapping is to solve this problem.

The phase method is originally used to align two images captured by left and right cameras in binocular stereo vision system [11]–[13]. In the application of binocular stereo vision system, phase-based method is able to recover small displacement between two images with subpixel accuracy as the frequencies of images are rich and disparities between images are relatively small. However, in fingerprint registration situation, the application of phase method needs adjustment. Fingerprint image has strong local frequency corresponding to the frequency of local ridge line. In order to remove the background noises and extract the fingerprint phase, the Gabor filter frequency u_0 must be set to the same as the frequency of local ridge line. But when the distortion between input and reference fingerprints exceeds half of the period of the ridge line, the traditional phase method cannot correctly recover the spatial displacement since the phase difference is constrained in a single period $(-\pi, \pi]$. To overcome this disadvantage, we can remove the constraint $(-\pi, \pi]$ on phases so that phases are no longer limited and can change continuously. This method calls phase unwrapping, or phase tracking, which refers to the reconstruction of the continuous phase from the wrapped phase by adding or subtracting $2n\pi$ at certain locations [19].

We hereby consider one-dimensional signal to demonstrate the concept of phase unwrapping. For a 1-D signal $y = f(n), n = 0, ..., N$, we can get its wrapped phase $\phi(n), n = 0, \ldots, N$ through Gabor filtering and four quadrant arctangent operation as mentioned in Section II-B. Then we start phase unwrapping to obtain the unwrapped phase $\phi_u(n), n = 0, \ldots, N$. As the beginning $n = 0$, we can directly set $\phi_u(x_0)$ equals to $\phi(x_0)$, and for its right neighbor x_1, its unwrapped phase $\phi_u(x_1)$ can be computed through:

$$\phi_u(x_1) = \phi(x_1) + \Delta\phi, \tag{14}$$

where

$$\Delta\phi = \begin{cases} \phi(x_1) - \phi(x_0) - 2\pi, & \text{if } \phi(x_1) - \phi(x_0) > \pi, \\ \phi(x_1) - \phi(x_0) + 2\pi, & \text{if } \phi(x_1) - \phi(x_0) \le -\pi, \\ \phi(x_1) - \phi(x_0), & \text{otherwise.} \end{cases} \tag{15}$$

The phase unwrapping result of 1-D signal is irrelevant to the sequence order of unwrapping. No matter starting from which position and along which direction, different unwrapping orders only lead to a global phase shift $d\phi$, which can be neglected by normalizing. However, in the application of 2-D fingerprint images, because there exists singular points

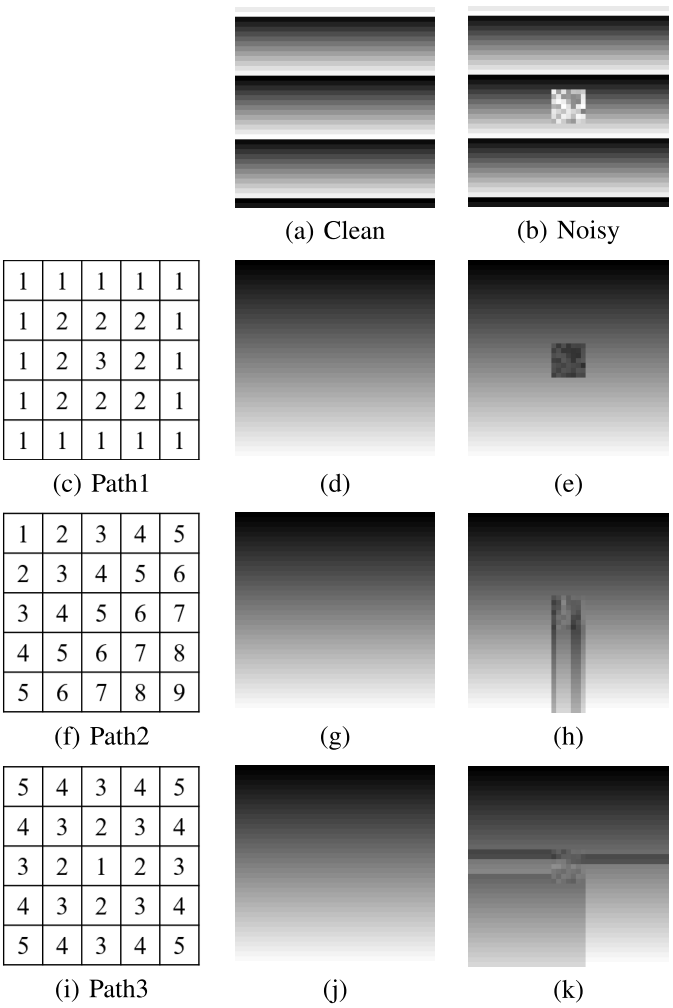

Fig. 6. 2-D phase unwrapping is path dependent for noisy image. (a) Clean image, (b) Noisy image, (c) Unwrapping path 1: from edges to center, (d) Unwrapped phase of clean image by path 1, (e) Unwrapped phase of noisy image by path 1, (f) Unwrapping path 2: from upper left corner to lower right corner, (g) Unwrapped phase of clean image by path 2, (h) Unwrapped phase of noisy image by path 2, (i) Unwrapping path 3: from center to corners, (j) Unwrapped phase of clean image by path 3, (k) Unwrapped phase of noise image by path 3.

and noises in fingerprint images, phase unwrapping result may rely on the unwrapping path. Fig. 6 shows how the unwrapping path affects the unwrapped phase of noisy image. (a) and (b) are the clean image and clean image having a noisy region in the center, (c)(f)(h) are three different unwrapping paths, and the numbers mean the unwrapping order, where regions of smaller number are unwrapped first. (d)(g)(j) are the corresponding unwrapped phases of clean image by three paths, and (e)(h)(k) are the unwrapped phases of noisy image. As we can see, the unwrapped phase of clean image is irrelevant of unwrapping paths, all three paths get the same result. However, the unwrapped phase of noisy image depends on the paths, incorrect path will lead to incorrect phase.

Therefore, we need to apply phase unwrapping method that are robust to noises. Researches have come up with a robust phase unwrapping method under the guidance of reliable judgment [20]. This method uses phase information

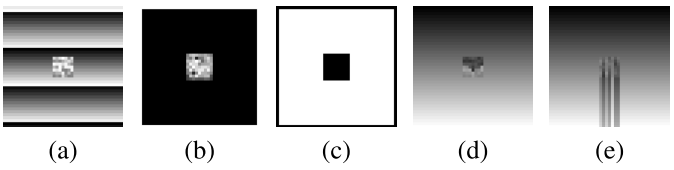

Fig. 7. Demonstration of robust unwrapping method. (a) Image with noise, (b) Second derivative of (a), (c) Reciprocal of (b), i.e. the reliance value, (d) Unwrapped phase by robust method, (e) Unwrapped phase by ordinary method.

of each pixel's neighborhood to calculate each pixel's reliance according to average gradient. Large gradient means that there may exist distortion near this position, thus this position is not reliable.

The usage of first-order gradient may have problems on continuously changing phases without noises. For example, $\phi_1(x, y) = x$ and $\phi_2(x, y) = 0.5x$ both don't have noises, thus they should be same reliable. However, after applying average gradient method along four directions, we can get $G_1(x, y) = 0.5$ and $G_2(x, y) = 0.25$. That is to say, $\phi_2(x, y)$ is more reliable than $\phi_1(x, y)$, which is obviously not realistic. To avoid this situation, we replace first-order average gradient with second-order average gradient along vertical, horizontal and two diagonal directions. Larger second-order average gradient means this pixel is less reliable, and we use its reciprocal to act as a reliable judgment:

$$R(x, y) = \frac{1}{G_2(x, y)}, \tag{16}$$

where $G_2(x, y)$ is the second-order average gradient at position (x, y). Fig. 7 illustrates that the usage of reliance measure can overcome noises and get the correct unwrapped phase. The five pictures are respectively the original images, the second derivative values, the reciprocals of second derivative, the unwrapped phases by robust method, the unwrapped phases by ordinary method. It is obvious that robust method deals with noisy region successfully and recovers the correct phases.

D. Distortion Estimation

According to the phase-shift principle of Fourier Transform, a spatial displacement Δx will lead to a corresponding phase shift $2\pi u_0 \Delta x$. Therefore, once having the phase shift $\Delta\phi$, we can further compute the spatial disparity at position (x, y):

$$d(x, y) = \frac{\Delta\phi(x, y)}{2\pi u_0}, \tag{17}$$

where u_0 is the frequency parameter of Gabor filter.

In 2-D situation, $d(x, y)$ is only the magnitude of spatial shift along the direction of Gabor filter or the new x', and we can get its components $d_x(x, y)$ and $d_y(x, y)$ along x and y directions through multiplying $\cos\theta$ and $\sin\theta$. Recalling Eq. 11, Eq. 17, and Fig. 5, we can get:

$$\begin{aligned} d_x(x, y) &= \frac{\Delta\phi(x, y)}{2\pi / P_R(x, y)} \cos(O_R(x, y) + \frac{\pi}{2}), \\ d_y(x, y) &= \frac{\Delta\phi(x, y)}{2\pi / P_R(x, y)} \sin(O_R(x, y) + \frac{\pi}{2}), \end{aligned} \tag{18}$$

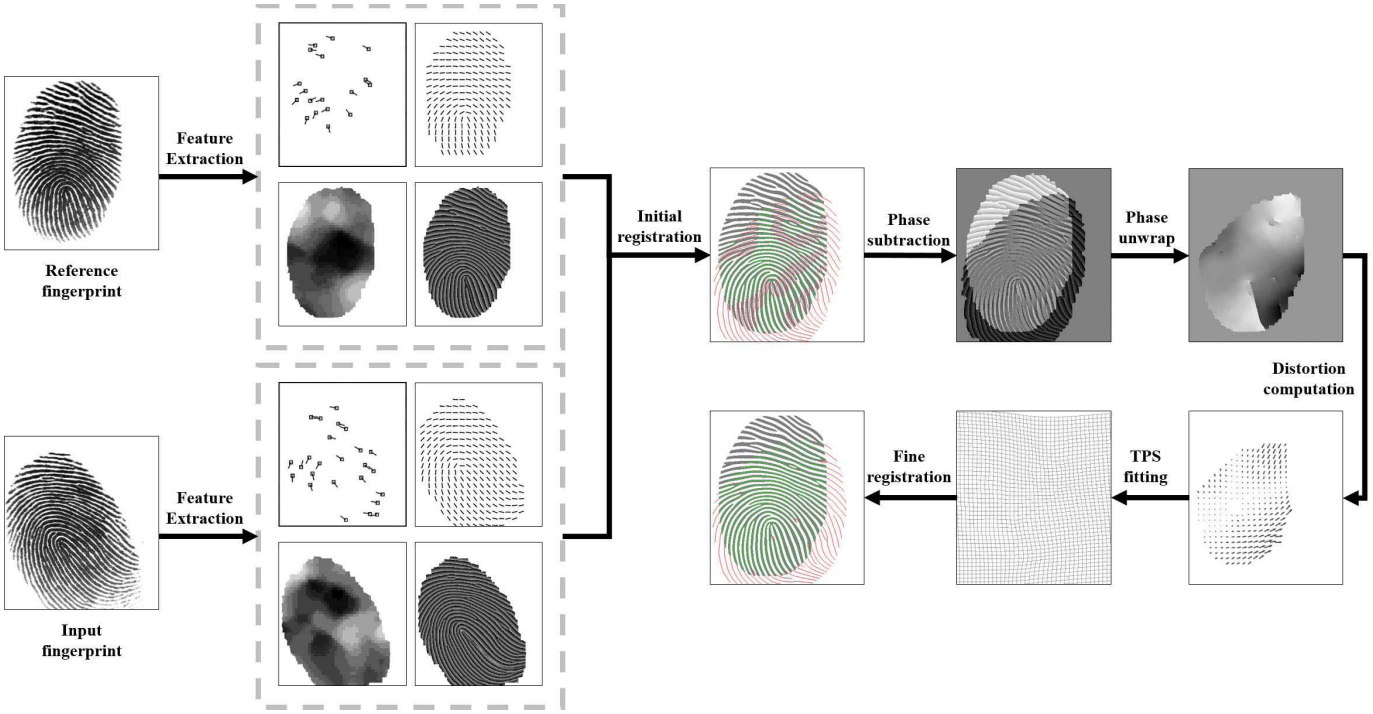

Fig. 8. Framework of phase registration scheme. In the registered images, the green lines highlight well registered ridges and the red lines indicate misaligned ridges or non-overlapping regions.

where P_R and O_R are the period map and orientation field of reference fingerprint.

III. Phase-Based Fingerprint Registration Algorithm

The approach described in Section II is not specific to fingerprint. In this section, we present the details which are specific to fingerprint registration. The proposed phase-based fingerprint registration algorithm is composed of four major parts: feature extraction, initial registration, phase subtraction and unwrapping, distortion field computation and fine registration. The framework of our algorithm is illustrated in Fig. 8.

A. Feature Extraction

In feature extraction step, conventional fingerprint features such as minutiae, orientation and period map are extracted from each fingerprint image using VeriFinger SDK 6.2 [21]. The wrapped phase is obtained through convolving the fingerprint image with 2-D Gabor filter $G(x, y)$, and taking the four quadrant arctangent function atan2(y, x) to get the phase. The orientation and frequency of Gabor filter $G(x, y)$ correspond to the values of local ridge line, as described in Eq. 11. Denote the image intensity as $I(x, y)$, then the wrapped phase Φ of fingerprint image can be computed as:

$$\Phi = \text{atan2}(\text{Re}[I * G], \text{Im}[I * G]). \tag{19}$$

Extracted features are shown in Fig. 9, including minutiae, orientation field and period map, real and imaginary components of filtered fingerprint image, amplitude and phase of filtered fingerprint image.

B. Initial Registration

The initial registration step, or coarse registration step, conducts global spatial transformation (rotation, translation, and distortion of certain degree) to coarsely align two fingerprints. In this step, first we use MCC minutia descriptor [22] to compute similarity between all possible minutiae pairs, and spectral clustering method [23] to find corresponding minutiae pairs between two fingerprints. MCC is the state-of-the-art minutiae descriptor, and spectral clustering is an effective and robust point matching technique in computer vision. Both algorithms are described in details in the original papers and there are SDK or code publicly available on the website. Then we use the matching pairs to act as landmarks points to fit a thin plate spline (TPS) transform model [24]. The TPS model is used to transform the input image and make it coarsely aligned with the reference fingerprint.

C. Phase Subtraction and Unwrapping

In section III-A, we have extracted the wrapped phase of input and reference fingerprints, then the subtraction step is quite simple. Due to the fact that not all minutiae pairs are perfectly aligned during the initial registration, phase subtraction result in areas around minutiae is unreliable. If the unreliable regions are visited early during unwrapping, the unwrapped phase may have deviations, leading to incorrect spatial distortion computation. Therefore, the subtracted phase is unwrapped based on noise-resistant phase unwrapping method introduced in Section II-C. A reliability value for each position is calculated, and positions with higher reliability are used first in unwrapping.

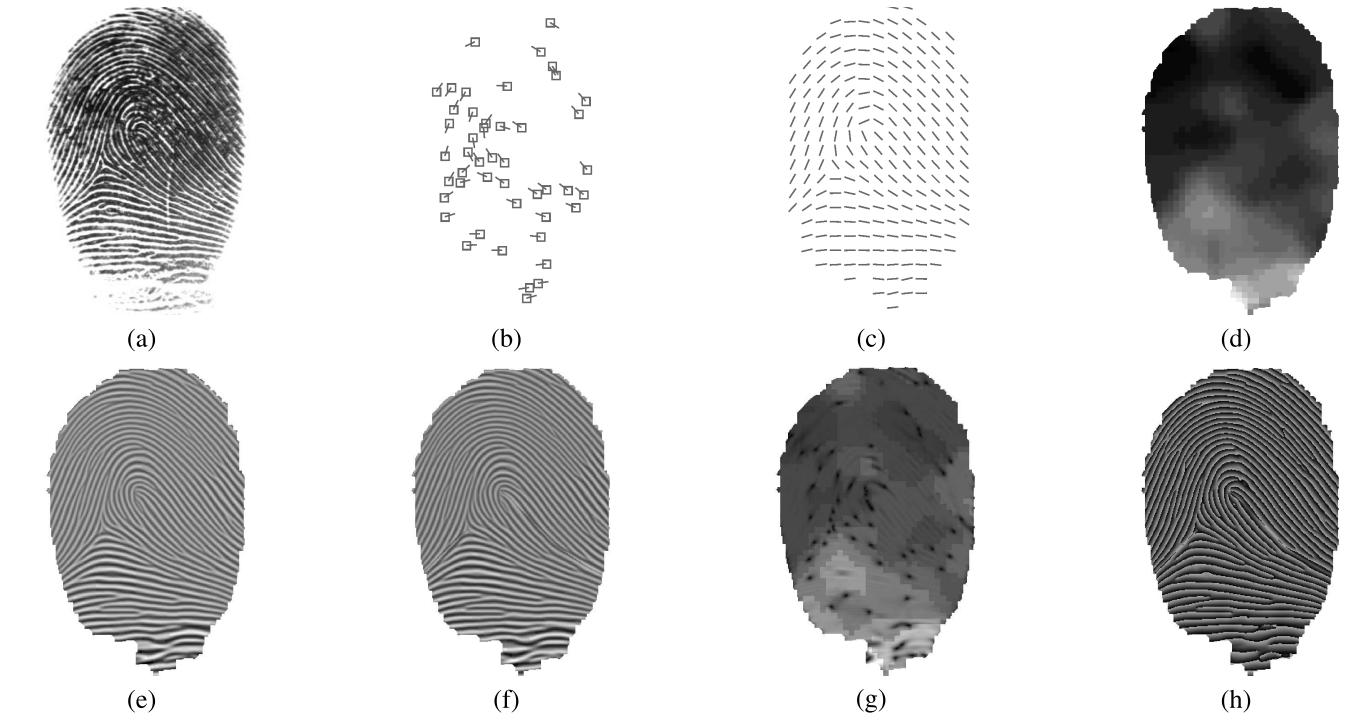

Fig. 9. Features extracted from a fingerprint. (a) Original fingerprint image, (b) Minutiae, (c) Orientation field, (d) Period map, (e) Real component of filtered fingerprint image, (f) Imaginary component of filtered fingerprint image, (g) Amplitude of filtered fingerprint image, and (h) Phase of filtered fingerprint image.

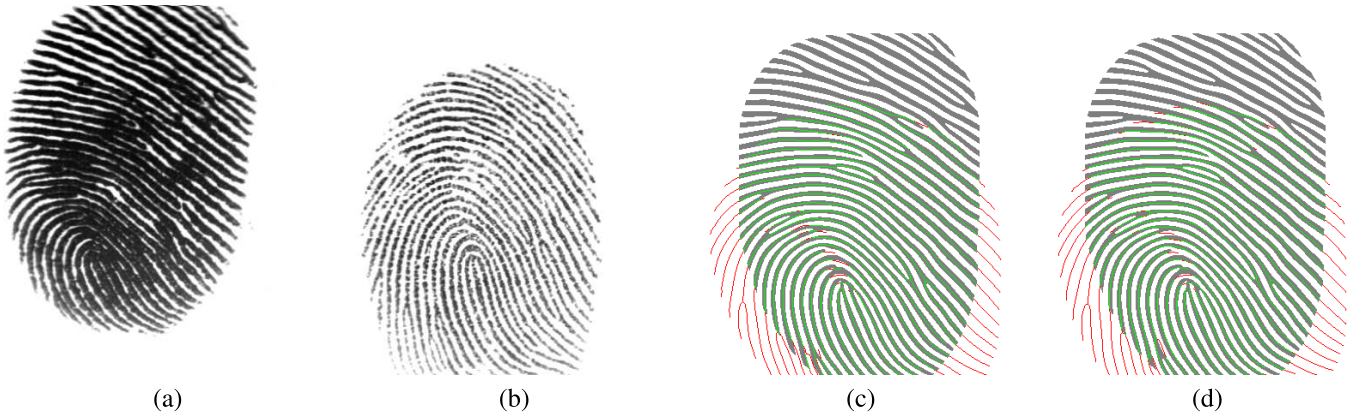

Fig. 10. Fine registration results of a pair of fingerprints with different sampling steps. (a) The input distorted fingerprint, (b) The reference fingerprint, (c) Fine registration with sampling step 13, (d) Fine registration with sampling step 28.

There exists two ways to compute the unwrapped phase difference between the input and reference fingerprints. One is to first unwrap the phase of the two fingerprints separately and then compute the phase difference. The other is to subtract the wrapped phase of the two fingerprints, and then unwrap the phase difference, which only requires doing unwrapping once. Obviously, the latter is better in efficiency and is adopted in the algorithm.

D. Distortion Field Computation and Fine Registration

After phase subtraction and unwrapping, the distortion field can be computed through Eq. 17 and 18 based on period map and orientation field, including shift magnitude $d(x, y)$ and its components d_x and d_y.

Given the fact that distortion is continuous and changes slowly, the outliers which deviate from neighboring points larger than a cut off value in the distortion field are removed to make our algorithm robust. Since the distortion is computed using phase demodulation other than image correlation or other feature matching methods, the proposed registration algorithm can achieve subpixel accuracy with low computational cost.

Meanwhile, we can uniformly sample on the distortion field in both horizontal and vertical directions to generate multiple correspondences between input and reference fingerprints. Since the distortion field has no abrupt change, sampling can speed up the algorithm, and does no harm to the accuracy. These generated matching pairs are treated as landmarks to the TPS fitting, and this registration aligns

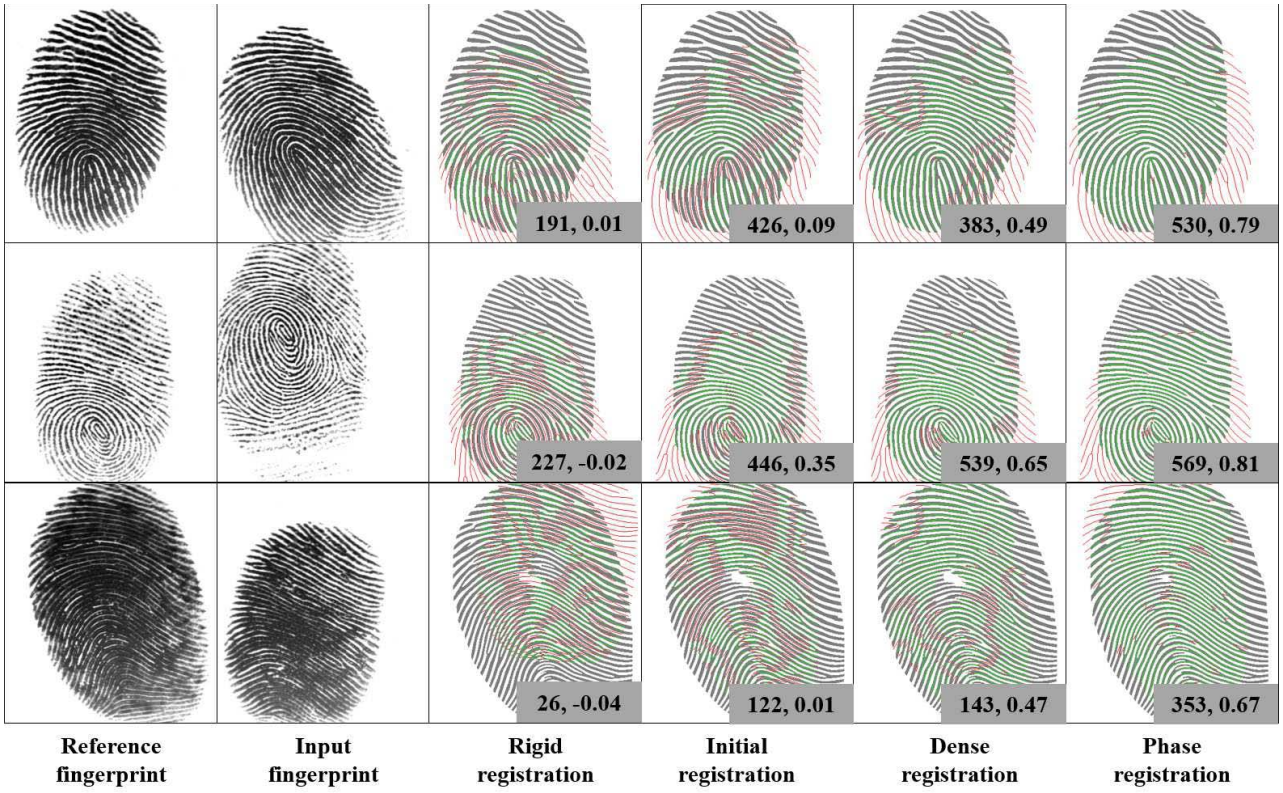

(a)

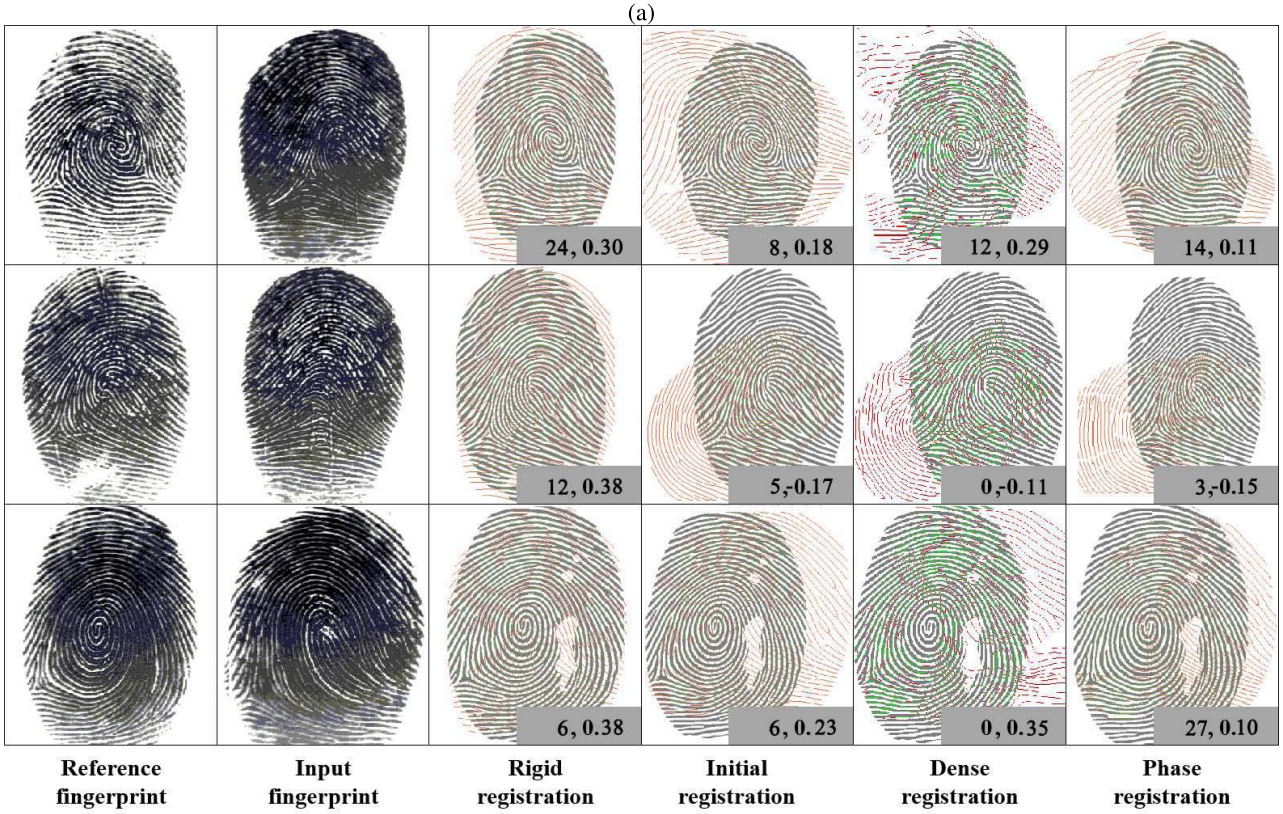

(b)

Fig. 11. Registration results of 4 different methods for 3 pairs of mated fingerprints and 3 pairs of non-mated fingerprints. (a) Genuine matching. (b) Impostor matching.

fingerprints better than initial registration. Fig. 10 shows results of different sampling steps, (c) is the registration result with sampling step 13, and (d) is the registration result with sampling step 28. Both registration results are comparable, but larger sampling step can efficiently accelerate the algorithm.

IV. Experiment

A. Databases

The proposed algorithm has been tested on FVC2004, TDF and NIST SD27 databases. FVC2004 consists of 4 sub-databases (DB), and each DB is composed of 800 images captured from 100 fingerprints. FVC2004 is one of the most challenging fingerprint databases, and a large proportion of fingerprints in this database are distorted. TDF consists of 320 pairs of distorted and mated normal fingerprints, in which 120 pairs of fingerprints have manually marked corresponding points. NIST SD27 contains 258 pairs of latent and rolled fingerprints.

B. Registration Accuracy

We compare the proposed phase registration method against 1) minutiae-based rigid registration [3], 2) minutiae-based TPS registration (i.e. the initial registration), and 3) image-based dense registration in [9], as well as original images without transformation. The first two baseline algorithms fit different transformation models to minutiae correspondences. The minutiae correspondences are generated by a matching algorithm which uses MCC-based local matching [22] and spectral clustering based global matching [23], as introduced in III-B. The third baseline algorithm, dense registration algorithm, is the first and only fingerprint registration algorithm which establishes dense correspondences, and has been thoroughly tested on public domain databases.

Registration examples of genuine and impostor matching from FVC2004 DB1_A are given in Fig. 11. Each row corresponds to a pair of input and reference fingerprints. The six columns are reference fingerprint, input fingerprint, rigid registration result, initial registration result, dense registration result, and the proposed phase registration result. The registration results are visualized by overlaying the thinned image of the registered input fingerprint on top of the binary image of the reference fingerprint. Green lines highlight well registered ridges, and red lines indicate misaligned ridges or non-overlapping region. The two numbers in the lower right corner of each registration result are the matching score of VeriFinger, and the correlation coefficient between the registered input fingerprint and reference fingerprint. Higher scores and coefficients indicate better registration results.

The genuine examples show that our phase-based registration algorithm registers all the ridges in the overlapped area correctly and has the highest matching score and correlation coefficient among all methods. Rigid registration algorithm roughly aligns two fingerprints since it can't handle nonlinear distortion, therefore, it has the worst result. Initial registration can correctly align ridges near minutiae correspondences, but fails in regions without minutiae pairs. Dense registration method works well on most areas of the fingerprints correctly, but works poorly near the border and noisy regions. And from the impostor examples we can see that, our phase-based method acts stably not only on genuine matching fingerprints, but also on impostor matching fingerprints. The matching score and correlation coefficient of impostor matching fingerprints have no apparent increases in comparison with genuine matching fingerprints.

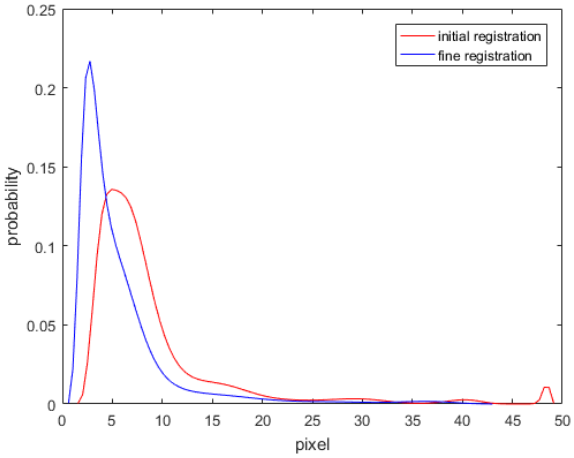

Fig. 12. Registration error distribution on TDF database using initial (red) and fine (blue) registration.

In order to measure the accuracy of our phase-based registration method, we test our method on TDF database, and compare the registered results with the manually registered ground truth. Fig. 12 shows the distance distribution of registered fingerprints from the ground truth through initial registration in Section III-B and fine registration. The average distances of initial registration (red) and fine registration (blue) is 8.91 and 5.65. Therefore, the fine registration reduces displacement from true result.

C. Matching Accuracy

Since the purpose of registration is to remove distortion before fingerprint matching, in order to quantitatively evaluate the impact of registration on matching accuracy, we conduct matching experiments on FVC2004 using registered fingerprints through different registration algorithms, where three subset databases DB1/2/3_A are tested (except DB4 synthetic fingerprint). We use image correlator and VeriFinger SDK 6.2 as fingerprint matchers.

The Detection Error Tradeoff (DET) curves of image correlator and VeriFinger matcher with different registration algorithms on FVC2004 DB1/2/3_A are shown in Fig. 13, which indicates that our phase-based method proves to be the best. Our phase-based method can register genuine matching fingerprints and achieve high correlation coefficients, while the coefficients of impostor matching fingerprints improve little after registration according to Fig. 13 a/c/e. And the DET curves of VeriFinger matcher after registration by different algorithms shown in Fig. 13 b/d/f show that phase registration method achieves the highest matching accuracy, which is consistent with the results from Fig. 11. The equal error rate (EER) of the proposed algorithm is 1.68%, which is better than the best matcher reported in [14] with an EER of 1.97%.

Fig. 14 displays the image correlation coefficient distributions of genuine and impostor matching by different registration algorithms on FVC2004 DB1_A. From the

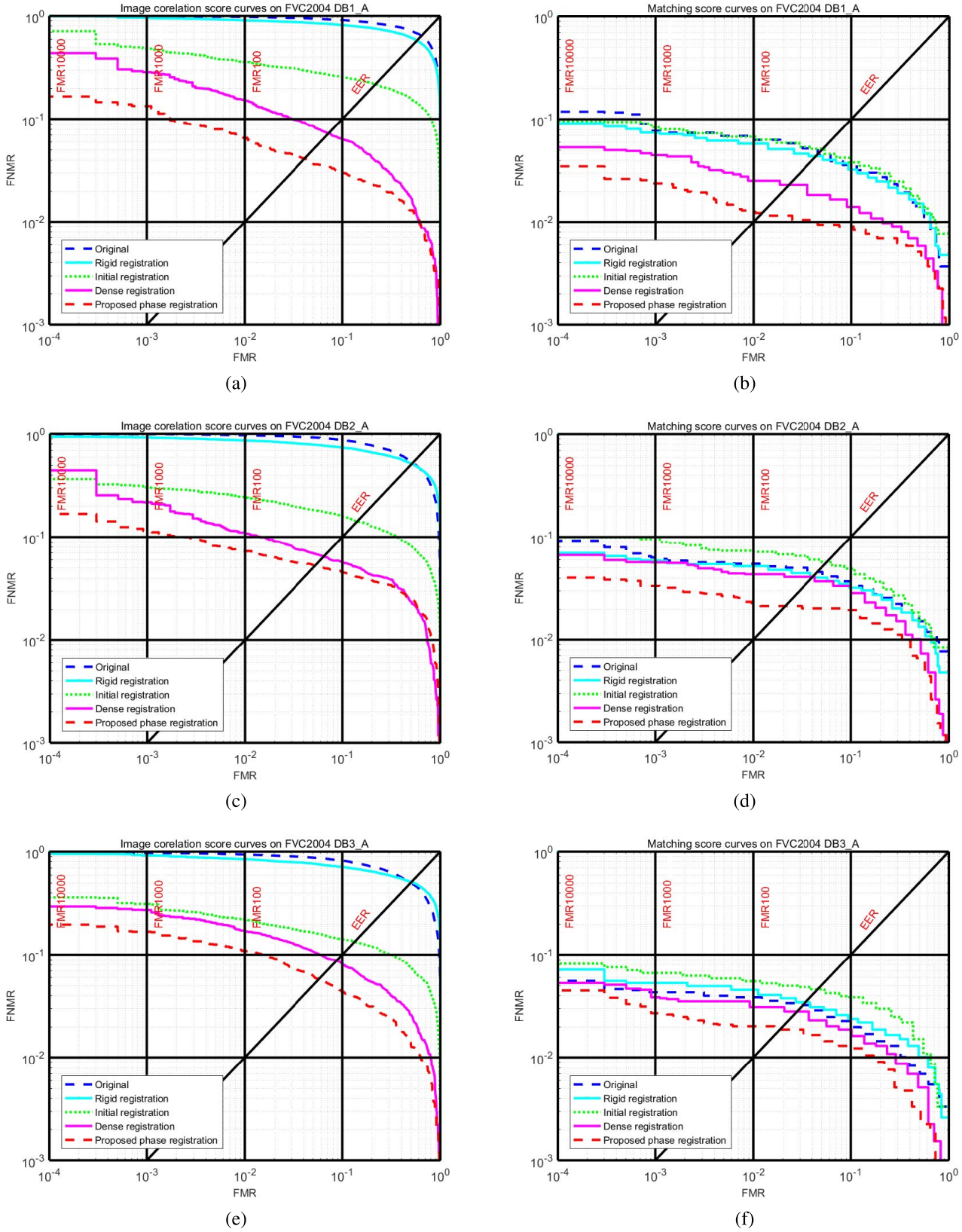

Fig. 13. DET curves of image correlator and VeriFinger matcher with different registration algorithms on FVC2004 DB1/2/3_A. (a) Image correlator on DB1_A. (b) VeriFinger matcher on DB1_A. (c) Image correlator on DB2_A. (d) VeriFinger matcher on DB2_A. (e) Image correlator on DB3_A. (f) VeriFinger matcher on DB3_A.

distribution curves we can see that both dense registration and our phase registration methods improve the genuine matching correlation coefficients as well as separating genuine and impostor matching, while other methods cannot distinguish genuine matching from impostor matching. It is also obvious from image correlation distribution that our phase method

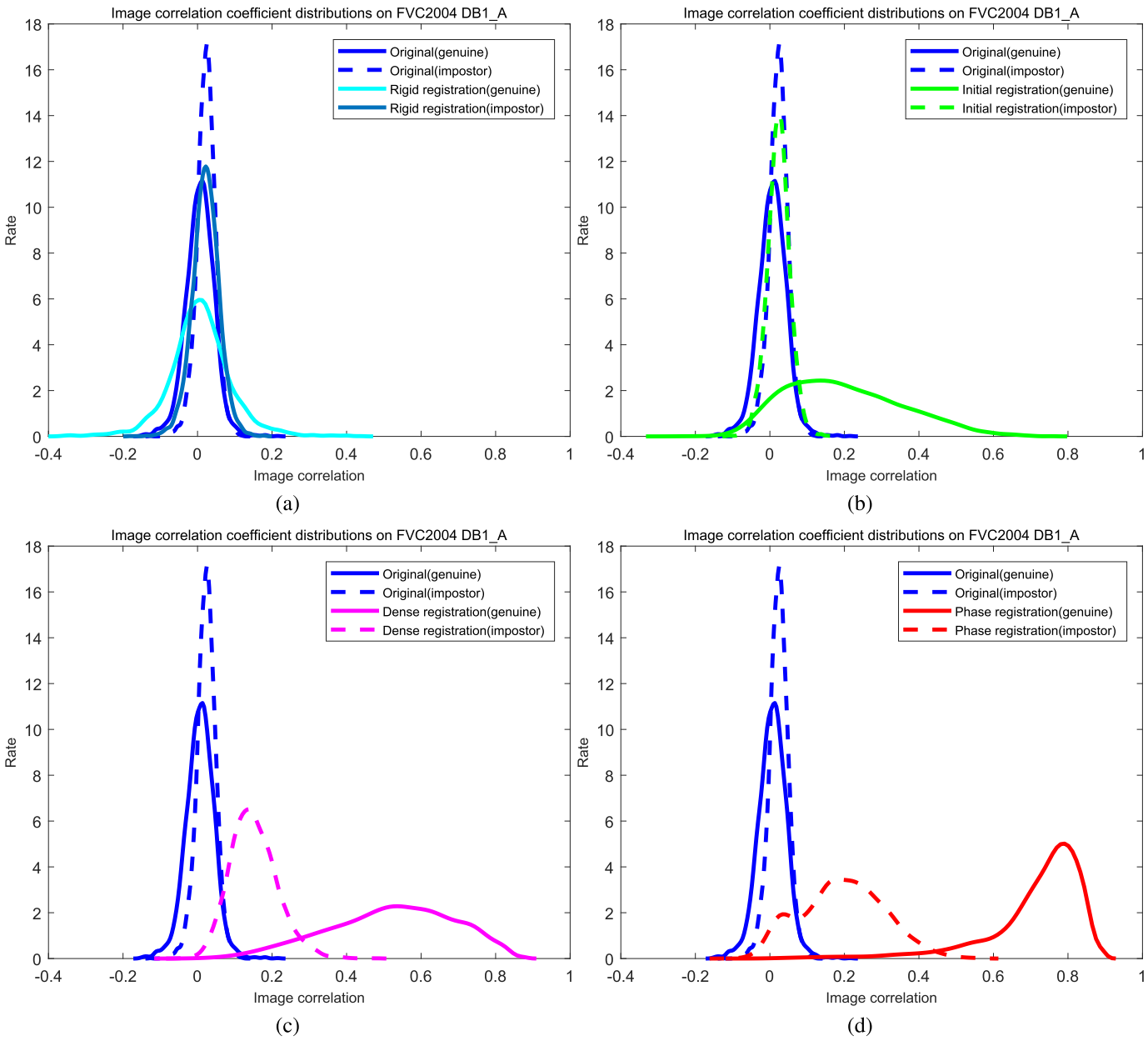

Fig. 14. Image correlation coefficient distributions of genuine and impostor matching by four different registration algorithms on FVC2004 DB1_A. (a) Rigid registration. (b) Initial registration. (c) Dense registration. (d) Phase registration.

performs better than dense registration, as reflected by smaller overlapping area between genuine and impostor distributions.

To examine the robustness of the proposed algorithm further, we conduct matching experiments on NIST SD27, and use Cumulative Match Characteristic (CMC) curve to describe the matching result. NIST SD27 contains 258 pairs of latent and corresponding rolled fingerprints, and we match them all, which generates 258×258 pairs of matching. We evaluate the matching result using VeriFinger matcher and image correlator the same as we use on FVC2004. The raw fingerprints are first enhanced through the newly-proposed FingerNet [25], which have shown effectiveness by applying deep learning in fingerprint processing. Then they are registered through different registration methods and matched by two matchers. According to Fig. 15, we can see that the proposed phase registration method reaches the highest identification rate among all registration algorithms.

D. Efficiency

The proposed phase registration method on distorted fingerprints is implemented in C and MATLAB code. Computing wrapped phase using Gabor filter, getting the period map, phase unwrapping, and TPS fitting and transformation are implemented in C, while other parts of the algorithm are implemented in MATLAB. The average time cost of the proposed algorithm is 1.99s on Intel Xeon E5-2640 2.5GHz CPU, including 0.38s for initial registration, 0.64s for phase unwrapping, 0.52s for distortion field computation, and 0.45s for TPS transformation. The average time cost of our phase method is faster than dense registration method, which is

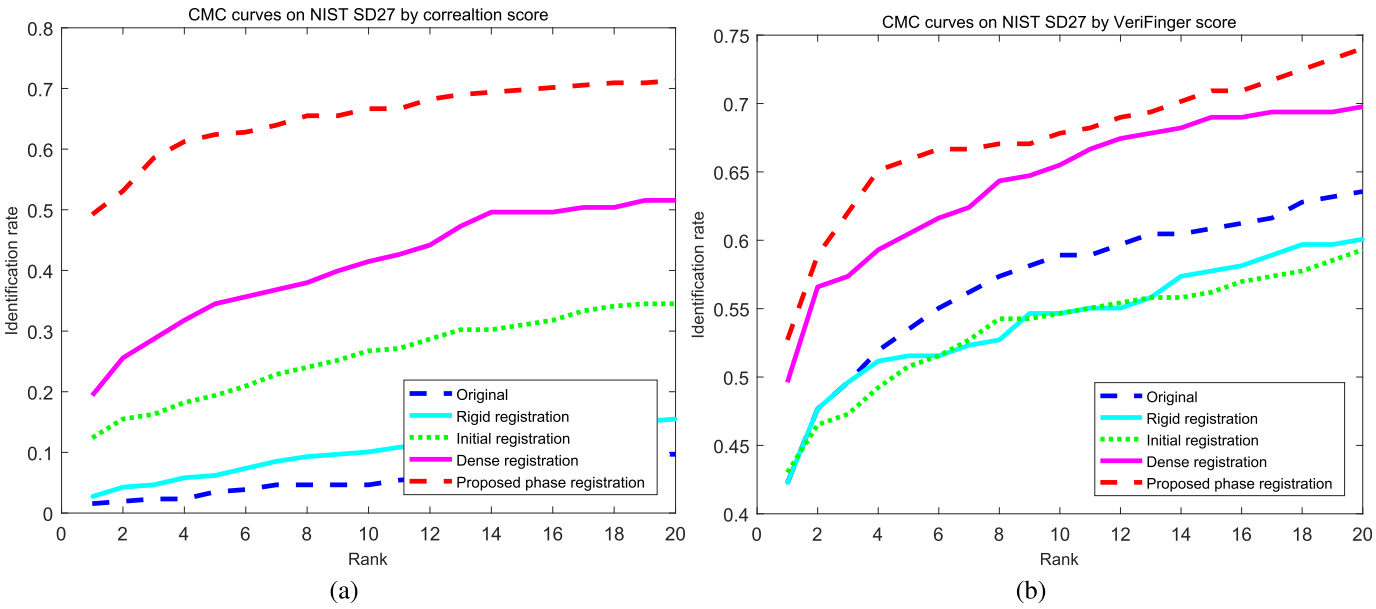

Fig. 15. CMC curves of image correlator and VeriFinger matcher with different registration algorithms on NIST SD27. (a) Image correlator on NIST SD27. (b) VeriFinger matcher on NIST SD27.

about 3s on FVC2004 DB1_A reported in [9]. Therefore, the proposed phase-based method is more efficient.

In Section III-D, we have mentioned that sampling on distortion field can speed up the algorithm, and we roughly try several sampling steps and their TPS fitting time cost. When the sampling step is set to 13 pixels, TPS fitting would cost 9.5s. However, when the sampling step is set to 28 pixels, TPS's time cost drops to 0.5s with barely no damage to fitting accuracy.

V. Conclusion

In this paper, we developed a phase-based fingerprint registration method by extending the method of phase demodulation from communication area. The proposed method first extracts traditional fingerprint features as well as phase features on both input and reference fingerprints, then performs an initial registration using minutiae correspondences and TPS fitting. Next, the method computes phase difference between input and reference fingerprints and do the phase unwrapping, which is the key to our phase-based method, as well as the following distortion field computation relying on unwrapped phases. Finally, we sample on the distortion field and fit a TPS model for fine registration.

Experiment results show that our phase-based fingerprint registration method outperforms other registration method both on registration accuracy and matching accuracy. Experiments on FVC2004, TDF, and NIST SD27 database indicate that our method produces more precise registration and better matching result on distorted fingerprints.

Meanwhile, the proposed phase-based registration method still meets challenge on latent fingerprint because of its large distortion and low fingerprint quality. Future work will explore the improvement on latent fingerprints.

References

[1] D. Maltoni, D. Maio, A. K. Jain, and S. Prabhakar, *Handbook of Fingerprint Recognition*. New York, NY, USA: Springer-Verlag, 2009.

[2] R. Cappelli, D. Maio, D. Maltoni, J. L. Wayman, and A. K. Jain, "Performance evaluation of fingerprint verification systems," *IEEE Trans. Pattern Anal. Mach. Intell.*, vol. 28, no. 1, pp. 3–18, Jan. 2006.

[3] M. Tico and P. Kuosmanen, "Fingerprint matching using an orientation-based minutia descriptor," *IEEE Trans. Pattern Anal. Mach. Intell.*, vol. 25, no. 8, pp. 1009–1014, Aug. 2003.

[4] H. Ramoser, B. Wachmann, and H. Bischof, "Efficient alignment of fingerprint images," in *Proc. 16th Int. Conf. Pattern Recognit.*, 2002, pp. 748–751.

[5] N. Yager and A. Amin, "Evaluation of fingerprint orientation field registration algorithms," in *Proc. 17th Int. Conf. Pattern Recognit.*, vol. 4, Aug. 2004, pp. 641–644.

[6] A. M. Bazen and S. H. Gerez, "Fingerprint matching by thin-plate spline modelling of elastic deformations," *Pattern Recognit.*, vol. 36, no. 8, pp. 1859–1867, 2003.

[7] A. Ross, S. Dass, and J. Anil, "A deformable model for fingerprint matching," *Pattern Recognit.*, vol. 38, no. 1, pp. 95–103, 2005.

[8] A. Ross, S. C. Dass, and A. K. Jain, "Fingerprint warping using ridge curve correspondences," *IEEE Trans. Pattern Anal. Mach. Intell.*, vol. 28, no. 1, pp. 19–30, Jan. 2006.

[9] X. Si, J. Feng, B. Yuan, and J. Zhou, "Dense registration of fingerprints," *Pattern Recognit.*, vol. 63, pp. 87–101, Mar. 2017.

[10] J. B. Anderson, T. Aulin, and C.-E. Sundberg, *Digital Phase Modulation*. New York, NY, USA: Springer, 1986.

[11] T. D. Sanger, "Stereo disparity computation using Gabor filters," *Biol. Cybern.*, vol. 50, no. 6, pp. 405–418, 1988.

[12] A. D. Jepson and M. R. M. Jenkin, "The fast computation of disparity from phase differences," in *Proc. IEEE Comput. Soc. Conf. Comput. Vis. Pattern Recognit.*, Jun. 1989, pp. 398–403.

[13] D. J. Fleet, A. D. Jepson, and M. R. M. Jenkin, "Phase-based disparity measurement," *CVGIP, Image Understand.*, vol. 53, no. 2, pp. 198–210, 1991.

[14] *FVC2004: The Third International Fingerprint Verification Competition*. Accessed: Jun. 5, 2018. [Online]. Available: http://bias.csr.unibo.it/fvc2004/

[15] E. De Castro and C. Morandi, "Registration of translated and rotated images using finite Fourier transforms," *IEEE Trans. Pattern Anal. Mach. Intell.*, vol. TPAMI-9, no. 5, pp. 700–703, Sep. 1987.

[16] R. Bracewell, *The Fourier Transform & Its Applications*. New York, NY, USA: McGraw-Hill, 1986.

[17] K. G. Larkin and P. A. Fletcher, "A coherent framework for fingerprint analysis: Are fingerprints holograms?" *Opt. Express*, vol. 15, no. 14, pp. 8667–8677, 2007.

[18] J. G. Daugman, "Uncertainty relation for resolution in space, spatial frequency, and orientation optimized by two-dimensional visual cortical filters," *J. Opt. Soc. Amer. A, Opt. Image Sci.*, vol. 2, no. 7, pp. 1160–1169, 1985.

[19] K. Itoh, "Analysis of the phase unwrapping algorithm," *Appl. Opt.*, vol. 21, no. 14, p. 2470, 1982.
[20] M. A. Herráez, D. R. Burton, M. J. Lalor, and M. A. Gdeisat, "Fast two-dimensional phase-unwrapping algorithm based on sorting by reliability following a noncontinuous path," *Appl. Opt.*, vol. 41, no. 35, pp. 7437–7444, 2002.
[21] Neurotechnology Inc. *VeriFinger SDK 6.2*. Accessed: Jun. 5, 2018. [Online]. Available: http://www.neurotechnology.com
[22] R. Cappelli, M. Ferrara, and D. Maltoni, "Minutia cylinder-code: A new representation and matching technique for fingerprint recognition," *IEEE Trans. Pattern Anal. Mach. Intell.*, vol. 32, no. 12, pp. 2128–2141, Dec. 2010.
[23] M. Leordeanu and M. Hebert, "A spectral technique for correspondence problems using pairwise constraints," in *Proc. IEEE Int. Conf. Comput. Vis.*, vol. 2, Oct. 2005, pp. 1482–1489.
[24] F. L. Bookstein, "Principal warps: Thin-plate splines and the decomposition of deformations," *IEEE Trans. Pattern Anal. Mach. Intell.*, vol. 11, no. 6, pp. 567–585, Jun. 1989.
[25] Y. Tang, F. Gao, J. Feng, and Y. Liu, "FingerNet: An unified deep network for fingerprint minutiae extraction," in *Proc. IEEE Int. Joint Conf. Biometrics*, Oct. 2017, pp. 108–116.

Zhe Cui received the B.S. degree from the Department of Physics, Tsinghua University, Beijing, China, in 2014, and the M.Eng. degree from the Department of Automation, Tsinghua University, in 2017, where he is currently pursuing the Ph.D. degree. His research interests include fingerprint recognition, computer vision, and pattern recognition.

Jianjiang Feng received the B.Eng. and Ph.D. degrees from the School of Telecommunication Engineering, Beijing University of Posts and Telecommunications, China, in 2000 and 2007, respectively. From 2008 to 2009, he was a Post-Doctoral Researcher with the PRIP Laboratory, Michigan State University. He is currently an Associate Professor with the Department of Automation, Tsinghua University, Beijing. His research interests include fingerprint recognition and computer vision. He is an Associate Editor of *Image and Vision Computing*.

Shihao Li received the B.Eng. and M.Eng. degrees from the Department of Automation, Tsinghua University, Beijing, China, in 2014 and 2017, respectively. He is currently with Alibaba Beijing.

Jiwen Lu received the B.Eng. degree in mechanical engineering and the M.Eng. degree in electrical engineering from the Xi'an University of Technology, Xi'an, China, in 2003 and 2006, respectively, and the Ph.D. degree in electrical engineering from Nanyang Technological University, Singapore, in 2012. He is currently an Associate Professor with the Department of Automation, Tsinghua University, Beijing, China. His current research interests include computer vision, pattern recognition, and machine learning. He has authored or co-authored over 190 scientific papers in these areas, where 54 of them are IEEE TRANSACTIONS papers and 32 of them are CVPR/ICCV/ECCV/NIPS papers. He is a member of the Multimedia Signal Processing Technical Committee and the Information Forensics and Security Technical Committee of the IEEE Signal Processing Society and a member of the Multimedia Systems and Applications Technical Committee of the IEEE Circuits and Systems Society. He was a recipient of the National 1000 Young Talents Plan Program in 2015. He served as the workshop chair/special session chair/area chair for more than 20 international conferences. He served as an Associate Editor for the IEEE TRANSACTIONS ON CIRCUITS AND SYSTEMS FOR VIDEO TECHNOLOGY, *Pattern Recognition*, and the *Journal of Visual Communication and Image Representation*. He also served as an Associate Editor for IEEE ACCESS, *Pattern Recognition Letters*, and *Neurocomputing*. He served as a guest editor for five special issues in international journals.

Jie Zhou received the B.S. and M.S. degrees from the Department of Mathematics, Nankai University, Tianjin, China, in 1990 and 1992, respectively, and the Ph.D. degree from the Institute of Pattern Recognition and Artificial Intelligence, Huazhong University of Science and Technology, Wuhan, China, in 1995. From 1995 to 1997, he was a Post-Doctoral Fellow with the Department of Automation, Tsinghua University, Beijing, China. Since 2003, he has been a Full Professor with the Department of Automation, Tsinghua University. In recent years, he has authored over 100 papers in peer-reviewed journals and conferences. Among them, over 40 papers have been published in top journals and conferences, such as the IEEE PAMI, TIP, and CVPR. His current research interests include computer vision, pattern recognition, and image processing. He was a recipient of the National Outstanding Youth Foundation of China Award. He is an Associate Editor of the IEEE TRANSACTIONS ON PATTERN ANALYSIS AND MACHINE INTELLIGENCE, the *International Journal of Robotics and Automation*, and two other journals.